

Revisiting and Advancing Fast Adversarial Training Through The Lens of Bi-Level Optimization

Yihua Zhang^{1,*} Guanhua Zhang^{2,*} Prashant Khanduri³ Mingyi Hong³
Shiyu Chang^{2,4} Sijia Liu^{1,4}

¹Computer Science & Engineering, Michigan State University, USA

²Computer Science, University of California, Santa Barbara

³Electrical & Computer Engineering, University of Minnesota

⁴MIT-IBM Watson AI Lab

* Equal contribution

May 16, 2022

Abstract

Adversarial training (AT) has become a widely recognized defense mechanism to improve the robustness of deep neural networks against adversarial attacks. It solves a min-max optimization problem, where the minimizer (*i.e.*, defender) seeks a robust model to minimize the worst-case training loss in the presence of adversarial examples crafted by the maximizer (*i.e.*, attacker). However, the min-max nature makes AT computationally intensive and thus difficult to scale. Meanwhile, the FAST-AT algorithm [1], and in fact many recent algorithms that improve AT, simplify the min-max based AT by replacing its maximization step with the simple one-shot gradient sign based attack generation step. Although easy to implement, FAST-AT lacks theoretical guarantees, and its practical performance can be unsatisfactory, suffering from the *robustness catastrophic overfitting* when training with strong adversaries.

In this paper, we propose to design FAST-AT from the fresh perspective of bi-level optimization (BLO). We first make the key observation that the most commonly-used algorithmic specification of FAST-AT is equivalent to using some gradient descent-type algorithm to solve a bi-level problem involving a sign operation. However, the discrete nature of the sign operation makes it difficult to understand the algorithm performance. Based on the above observation, we propose a new tractable bi-level optimization problem, and design and analyze a new set of algorithms termed Fast Bi-level AT (FAST-BAT). In contrast to FAST-AT, FAST-BAT is capable of defending sign-based projected gradient descent (PGD) attacks without calling any gradient sign method and explicit robust regularization during training. Furthermore, we empirically show that our method outperforms state-of-the-art FAST-AT baselines, by achieving superior model robustness without inducing robustness catastrophic overfitting, or suffering from any loss of standard accuracy.

1 Introduction

Given the fact that machine learning (ML) models can be easily fooled by tiny adversarial perturbations (also known as adversarial attacks) on the input [2–4], learning robust deep neural networks (DNNs) is now a major focus in research. Nearly all existing effective defense mechanisms [5–7, 1, 8, 9] are built on the adversarial training (AT) recipe, first developed in [10] and later formalized in [5] using min-max optimization. In contrast to standard model training using empirical risk minimization, AT [5] calls *min-max optimization*. That is, a minimizer (*i.e.* defender) seeks to update model parameters against a maximizer (*i.e.* attacker) that aims to increase the training loss by perturbing each training example.

The AT-type defenses have been widely adopted in various application domains including image classification [2, 5, 11], object detection [12], natural language processing [13, 14], and healthcare [15, 16]. Despite their effectiveness, the min-max optimization nature makes them difficult to scale. This is because *multiple* maximization steps (required by an iterative attack generator) are needed at every model training step in AT. The resulting prohibitive computation cost makes AT not suitable in practical settings when computing resources are limited. For example, [17] used 128 GPUs to make AT practical on ImageNet. Thereby, how to speed up AT without losing accuracy and robustness is now a *grand challenge* for adversarial defense [1].

Recently, references [1, 7, 8, 18] attempted to develop computationally-efficient alternatives of AT, that is, the ‘fast’ versions of AT. To the best of our knowledge, FAST-AT [1] and FAST-AT with gradient alignment (GA) regularization, termed FAST-AT-GA [18], are the two state-of-the-art (SOTA) ‘fast’ versions of AT, since they achieve a significant reduction in computation complexity and preserve accuracy and robustness to some extent. To be specific, FAST-AT [1] replaces an iterative attack generator used in AT with a heuristic single-step attack generation method. Thus, its computation cost is as cheap as the standard model training. However, FAST-AT suffers from two main issues: (i) lack of stability, *i.e.*, it has a large variance in performance [19], and (ii) robustness catastrophic overfitting, *i.e.*, when training with strong adversaries, the robustness of the resulting model can drop significantly [18]. To alleviate these problems, [18] proposed FAST-AT-GA by penalizing FAST-AT using an explicit robust regularization given by GA. However, we will show that FAST-AT-GA encounters another problem (iii) FAST-AT-GA may sacrifice standard accuracy, achieving a poor accuracy-robustness tradeoff for large attack budget (e.g., $\epsilon = 16/255$ in Table 1), *i.e.*, the improvement of robust accuracy (RA) is at cost of a sharp drop in standard accuracy (SA). Moreover, (iv) there has been no theoretical guarantee of the optimization algorithms used in FAST-AT and FAST-AT-GA. Given the limitations (i)- (iv), we ask:

How to design a ‘fast’ version of AT with improved stability, mitigated catastrophic overfitting, enhanced accuracy-robustness tradeoff, and some theoretical guarantees?

To address the above question, in this paper we put forward a new perspective to the AT problem, that instead of treating it as a min-max problem, it should be formulated as a more general bi-level optimization (BLO) problem [20], where the attack generation problem is a *lower-level* optimization problem (possibly with constraints), while the defense is the *upper-level* optimization problem. To the best of our knowledge, this is the first work that makes a rigorous connection between adversarial defense and BLO. Technically, we show that FAST-AT can be *interpreted* as BLO with linearized lower-level problems. Delving into the linearization of BLO, we propose a novel, theoretically-grounded ‘fast’ AT framework, **fast bi-level AT** (FAST-BAT). Practically, Table 1 highlights some achieved improvements over FAST-AT and FAST-AT-GA: When a stronger train-time attack (*i.e.*, $\epsilon = 16/255$ vs. $8/255$) is adopted, FAST-AT suffers a large degradation of RA and SA, together with higher variances than proposed FAST-BAT. Although FAST-AT-GA outperforms FAST-AT, it still incurs a significant SA loss (over 21%) at $\epsilon = 16/255$. In contrast, FAST-BAT produces a more graceful SA-RA tradeoff: 9% improvement of SA without loss of RA. Further, compared with FAST-AT-GA, FAST-BAT is computationally much cheaper because no robust regularization is needed.

Table 1: Performance overview of proposed FAST-BAT vs. the baselines FAST-AT [1] and FAST-AT-GA [18] on (CIFAR-10, PreActResNet-18). All methods are robustly trained under two perturbation budgets $\epsilon = 8/255$ and $16/255$ over 20 epochs. We use the early-stopping policy [21] to report the model of best robustness for each method. The evaluation metrics include robust accuracy (RA) against PGD-50-10 attacks (50-step PGD attack with 10 restarts) [5] at $\epsilon = 8/255$ and $16/255$ (test-time ϵ is *same* as the train-time), RA against AutoAttack (AA) [22] at $\epsilon = 8/255$ and $16/255$, and computation time (per epoch). The result $a \pm b$ represents mean a and standard deviation b over 10 random trials. All experiments are run on a single Tesla-P100 GPU.

Method	RA-PGD (%) ($\epsilon = 8/255$)	RA-PGD (%) ($\epsilon = 16/255$)	RA-AA (%) ($\epsilon = 8/255$)	RA-AA (%) ($\epsilon = 16/255$)	SA (%) ($\epsilon = 8/255$)	SA (%) ($\epsilon = 16/255$)	Time (s)
FAST-AT	45.47 \pm 0.39	21.79 \pm 0.93	41.97 \pm 0.15	12.57 \pm 0.33	81.72 \pm 0.36	46.02 \pm 2.79	42
FAST-AT-GA	47.43 \pm 0.42	26.22 \pm 0.19	43.52 \pm 0.32	18.03 \pm 0.39	79.84 \pm 0.49	58.57 \pm 1.19	150
FAST-BAT	48.74 \pm 0.11	26.15 \pm 0.12	44.89 \pm 0.12	18.21 \pm 0.15	79.43 \pm 0.08	67.79 \pm 0.08	135

Contributions. The main contribution of this work is to propose a new formulation based on BLO, as well as a class of new algorithms termed FAST-BAT, for the adversarially robust training problem. The specific contributions are listed below:

① We show that the popular FAST-AT algorithm can be viewed as applying certain (stochastic) gradient methods for solving a special case of the proposed BLO formulation, which involves a discrete lower-level (*i.e.*, the adversary’s) objective function. This key observation not only provides a new interpretation of FAST-AT, but most importantly, it explains *why* FAST-AT may not possess strong theoretical guarantees (because of the involvement of the discrete objective function).

② Based on our new understanding of FAST-AT, as well as the insights gained from the recent advances in BLO, we then propose a new *smooth* objective for the lower-level problem. The desirable smoothness property

further enables us to design a novel bi-level optimization algorithm that is capable of computing a closed-form implicit gradient solution of the resulting problem.

③ We conduct extensive experiments on FAST-BAT, showing its improved stability, mitigated catastrophic overfitting, and enhanced accuracy-robustness tradeoff; see some illustrations in Table 1.

2 Related work

Adversarial attack. Adversarial attacks are techniques to generate malicious perturbations that are imperceptible to humans but can mislead the ML models [2, 3, 22–24]. A popular threat model that an adversary uses is known as ℓ_p -norm ball constrained attack ($p \in \{0, 1, 2, \infty\}$). This is also the focus of this paper. The adversarial attack has become a major approach to evaluate the robustness of deep neural networks (DNNs) and thus, help build safe artificial intelligence in many high-stakes applications such as autonomous driving [25, 26], surveillance [27, 28], and healthcare [15].

Adversarial defense and robust training at scale. Our work falls into the category of robust training, which was mostly built upon min-max optimization. For example, [5] established the framework of AT for the first time, which has been recognized as one of the most powerful defenses [9]. Extended from AT, TRADES [6] sought the optimal balance between robustness and generalization ability. Further, AT-type defense has been generalized to the semi-/self-supervised settings [29, 30] and integrated with certified defense techniques such as randomized smoothing [31].

Despite the effectiveness of AT and its variants, they require high computation costs. How to speed up AT without losing performance remains an open question. Some recent works attempted to impose algorithmic simplifications to AT, leading to *fast but approximate* AT algorithms, such as ‘free’ AT [7], you only propagate once (YOPO) [8], FAST-AT [1], and FAST-AT regularized by gradient alignment (termed FAST-AT-GA) [18]. In particular, FAST-AT and FAST-AT-GA are the baselines most relevant to ours since they were designed with the least computation complexity. However, their defense performance is far from satisfactory. For example, FAST-AT has poor training stability [19] and suffers catastrophic overfitting when facing strong attacks [18]. In contrast to FAST-AT, FAST-AT-GA yields improved robustness but has a poor accuracy-robustness tradeoff (e.g., Table 1). In this paper, we aim to advance the algorithm foundation of ‘fast robust training’ through the lens of BLO (bi-level optimization). We will show that the proposed FAST-BAT can lead to stable robust learning without suffering catastrophic overfitting and a graceful tradeoff between accuracy and robustness.

Bi-level optimization (BLO). BLO is a unified hierarchical learning framework, where the objective and variables of an upper-level problem depend on the optimizer of certain lower-level problems. The BLO problem in its most generic form is a class of very challenging problems, and thus, the design of algorithms and theory for BLO focuses on special cases [32–38]. In practice, some successful applications of BLO to ML have been witnessed in meta-learning [39], data poisoning attack design [40], and reinforcement learning [41]. However, as will be evident later, the existing BLO approach is not directly applied to adversarial defense due to the presence of the *constrained* nonconvex lower-level problem (for attack generation). To the best of our knowledge, our work makes a rigorous connection between adversarial defense and BLO for the first time.

3 A Bi-Level Optimization View on FAST-AT

Preliminaries on AT and FAST-AT. Let us consider the following standard min-max formulation for the robust adversarial training problem [5]

$$\underset{\theta}{\text{minimize}} \mathbb{E}_{(\mathbf{x}, y) \in \mathcal{D}} \left[\underset{\delta \in \mathcal{C}}{\text{maximize}} \ell_{\text{tr}}(\theta, \mathbf{x} + \delta, y) \right], \quad (1)$$

where $\theta \in \mathbb{R}^n$ denotes model parameters; \mathcal{D} is the training set consisting (a finite number) of labeled data pairs with feature \mathbf{x} and label y ; $\delta \in \mathbb{R}^d$ represents adversarial perturbations subject to the perturbation constraint \mathcal{C} , e.g., $\mathcal{C} = \{\delta \mid \|\delta\|_{\infty} \leq \epsilon, \delta \in [0, 1]\}$ for ϵ -toleration ℓ_{∞} -norm constrained attack (normalized to $[0, 1]$); $\ell_{\text{tr}}(\cdot)$ is the training loss. Using the above notation, $(\mathbf{x} + \delta)$ represents an adversarial example.

The standard solver for problem (1) is known as AT [5]. However, it has to call an *iterative* optimization method (e.g., K -step PGD attack) to solve the inner maximization problem of (1). As a result, AT is computationally expensive. To improve its scalability, the FAST-AT algorithm which only takes the *single-step* PGD attack for inner maximization was proposed and successfully implemented in [1]. The algorithm backbone of FAST-AT is summarized below.

FAST-AT algorithm

Let θ_t be the model parameters at iteration t . The $(t + 1)$ th iteration is given by

① (*Inner maximization by 1-step PGD*): $\delta \leftarrow \mathcal{P}_{\mathcal{C}}(\delta_0 + \alpha \cdot \text{sign}(\nabla_{\delta} \ell_{\text{tr}}(\theta_t, \mathbf{x} + \delta, y)))$, where $\mathcal{P}_{\mathcal{C}}(\mathbf{a})$ denotes the projection operation that projects the point \mathbf{a} onto \mathcal{C} , i.e., $\mathcal{P}_{\mathcal{C}}(\mathbf{z}) = \arg \min_{\delta \in \mathcal{C}} \|\delta - \mathbf{z}\|_2^2$, δ_0 is a random uniform initialization within $[0, 1]$, $\alpha > 0$ is a proper learning rate (e.g., 1.25ϵ), and $\text{sign}(\cdot)$ is the element-wise sign operation.

② (*Outer minimization for model training*): This can be conducted by any standard optimizer, e.g., SGD. That is, $\theta_{t+1} \leftarrow \theta_t - \beta \nabla_{\theta} \ell_{\text{tr}}(\theta_t, \mathbf{x} + \delta, y)$, where $\beta > 0$ is a proper learning rate (e.g., cyclic learning rate), and δ is provided from the inner maximization step.

In what follows, we provide a few remarks about FAST-AT listed in order.

First, roughly speaking, FAST-AT is a simplification of AT using 1-step PGD for inner maximization. However, it is not entirely clear which problem FAST-AT is actually solving. If we take a closer look at the algorithm, we will see that the inner update only changes to the *initial* δ_0 , not the most recent δ . Clearly, this scheme is fundamentally *different* from the classical gradient descent-ascent algorithm for min-max optimization (see, e.g., [42]), which alternately updates the inner and outer variables. Therefore it is not clear if FAST-AT is really solving the original min-max problem (1).

Second, as shown in [1], the successful implementation of FAST-AT needs sophisticated hyperparameter tuning for α , δ_0 , and β .

Third, despite the efficacy of FAST-AT in some cases, [18] demonstrated that it could lead to the issue of robustness catastrophic overfitting when facing strong adversaries during training. In the literature, there was no grounded theory to justify the pros and cons of FAST-AT. We will show that BLO provides a promising solution.

BLO: Towards a unified formulation of robust training. BLO (bi-level optimization) is an optimization problem that involves two levels of optimization tasks, where the *lower-level* task is nested inside the *upper-level* task. More precisely, it has the following generic form:

$$\begin{aligned} & \underset{\mathbf{u} \in \mathcal{U}}{\text{minimize}} && f(\mathbf{u}, \mathbf{v}^*(\mathbf{u})) \\ & \text{subject to} && \mathbf{v}^*(\mathbf{u}) = \arg \min_{\mathbf{v} \in \mathcal{V}} g(\mathbf{v}, \mathbf{u}) \end{aligned} \quad (2)$$

where \mathcal{U} and \mathcal{V} are the feasible sets for the variables \mathbf{u} and \mathbf{v} , respectively; $f(\cdot)$ and $g(\cdot)$ are the upper- and the lower-level objective functions, respectively. Intuitively, the BLO (2) can be used to formulate the adversarial training problem as the latter also involves two problems, one nested in the other. Importantly, it is more powerful than the min-max formulation (1) as it allows the two problems to have *different* objective functions. Later we will see that the flexibility provided by BLO is the key to the generality of our proposed framework.

To make the above intuition precise, we use the upper-level problem to model the training loss minimization, while the lower-level problem to model the attack generation process, and consider the following BLO problem:

$$\begin{aligned} & \underset{\theta}{\text{minimize}} && \mathbb{E}_{(\mathbf{x}, y) \in \mathcal{D}} [\ell_{\text{tr}}(\theta, \mathbf{x} + \delta^*(\theta; \mathbf{x}, y); y)] \\ & \text{subject to} && \delta^*(\theta; \mathbf{x}, y) = \arg \min_{\delta \in \mathcal{C}} \ell_{\text{atk}}(\theta, \delta; \mathbf{x}, y), \end{aligned} \quad (3)$$

where the training loss function $\ell_{\text{tr}}(\cdot)$ has been defined in (1), and $\ell_{\text{atk}}(\cdot)$ denotes an attack objective. For the notation simplicity, in the subsequent discussion we will not indicate the dependency of the functions ℓ_{tr} , ℓ_{atk} , and δ^* with respect to (w.r.t.) the data samples (\mathbf{x}, y) . The formulation (3) has two key differences from (1):

– First, when we choose $\ell_{\text{atk}} = -\ell_{\text{tr}}$, problem (3) becomes equivalent to the min-max formulation (1). It follows that the BLO is suitable to formulate the adversarial training problem. Moreover, we will see shortly that the flexibility provided by choosing the lower-level objective *independently* of the upper-level one enables us to interpret FAST-AT as solving a certain special form of the BLO problem. Note that prior to our work, it was not entirely clear what is the problem that FAST-AT algorithm is trying to solve (as mentioned above).

– Second, BLO calls an optimization routine that is different from those used to solve the min-max optimization problem (1), even when we set $\ell_{\text{atk}} = -\ell_{\text{tr}}$ (see further analysis in Appendix B). Specifically, for a given data sample (\mathbf{x}, y) , the stochastic gradient for the upper-level problem of (3) can be computed by

$$\frac{d\ell_{\text{tr}}(\boldsymbol{\theta}, \boldsymbol{\delta}^*(\boldsymbol{\theta}))}{d\boldsymbol{\theta}} = \nabla_{\boldsymbol{\theta}}\ell_{\text{tr}}(\boldsymbol{\theta}, \boldsymbol{\delta}^*(\boldsymbol{\theta})) + \underbrace{\frac{d\boldsymbol{\delta}^*(\boldsymbol{\theta})^\top}{d\boldsymbol{\theta}}}_{\text{IG}} \nabla_{\boldsymbol{\delta}}\ell_{\text{tr}}(\boldsymbol{\theta}, \boldsymbol{\delta}^*(\boldsymbol{\theta})), \quad (4)$$

where the superscript \top denotes the transpose operation, and $\nabla_{\boldsymbol{\theta}}\ell_{\text{tr}}(\boldsymbol{\theta}, \boldsymbol{\delta}^*(\boldsymbol{\theta}))$ denotes the partial derivative with respect to (w.r.t.) the first input argument $\boldsymbol{\theta}$; and $\frac{d\boldsymbol{\delta}^*(\boldsymbol{\theta})^\top}{d\boldsymbol{\theta}} \in \mathbb{R}^{n \times d}$, if exists, is referred to as *implicit gradient* (IG) because it is defined through an implicitly constrained optimization problem $\min_{\boldsymbol{\delta} \in \mathcal{C}} \ell_{\text{atk}}$. The dependence on IG is a ‘fingerprint’ of BLO (1) in contrast to AT or FAST-AT.

BLO-enabled interpretation of FAST-AT. In what follows, we demonstrate how FAST-AT relates to BLO. Our main finding is summarized below.

Bi-level interpretation of FAST-AT

FAST-AT can be interpreted as an approximated stochastic gradient algorithm for solving the following **lower-level linearized BLO**, with $\mathbf{z} = \boldsymbol{\delta}_0$ and $\lambda = 1/\alpha$:

$$\begin{aligned} & \underset{\boldsymbol{\theta}}{\text{minimize}} && \mathbb{E}_{(\mathbf{x}, y) \in \mathcal{D}}[\ell_{\text{tr}}(\boldsymbol{\theta}, \boldsymbol{\delta}^*(\boldsymbol{\theta}))] \\ & \text{subject to} && \boldsymbol{\delta}^*(\boldsymbol{\theta}) = \arg \min_{\boldsymbol{\delta} \in \mathcal{C}} [(\boldsymbol{\delta} - \mathbf{z})^\top \text{sign}(\nabla_{\boldsymbol{\delta}=\mathbf{z}}\ell_{\text{atk}}(\boldsymbol{\theta}, \boldsymbol{\delta})) + (\lambda/2)\|\boldsymbol{\delta} - \mathbf{z}\|_2^2], \end{aligned} \quad (5)$$

where \mathbf{z} is the linearization point, $\nabla_{\boldsymbol{\delta}=\mathbf{z}}\ell_{\text{atk}}$ denotes the partial derivative of ℓ_{atk} (w.r.t. $\boldsymbol{\delta}$) evaluated at \mathbf{z} , $\text{sign}(\nabla_{\boldsymbol{\delta}=\mathbf{z}}\ell_{\text{atk}}(\boldsymbol{\theta}, \boldsymbol{\delta}))$ is the linearization direction, and $\lambda > 0$ is a regularization parameter associated with the quadratic residual of linearization.

Our justification for the above claim is elaborated below.

– First, the simplified lower-level problem of (5) leads to the **closed-form** solution

$$\begin{aligned} \boldsymbol{\delta}^*(\boldsymbol{\theta}) &= \arg \min_{\boldsymbol{\delta} \in \mathcal{C}} (\lambda/2)\|\boldsymbol{\delta} - \mathbf{z} + (1/\lambda)\text{sign}(\nabla_{\boldsymbol{\delta}=\mathbf{z}}\ell_{\text{atk}}(\boldsymbol{\theta}, \boldsymbol{\delta}))\|_2^2 \\ &= \mathcal{P}_{\mathcal{C}}(\mathbf{z} - (1/\lambda)\text{sign}(\nabla_{\boldsymbol{\delta}=\mathbf{z}}\ell_{\text{atk}}(\boldsymbol{\theta}, \boldsymbol{\delta}))), \end{aligned} \quad (6)$$

which is given by the 1-step PGD attack with initialization \mathbf{z} and learning rate $(1/\lambda)$. In the linearization used in (5), a quadratic regularization term (with regularization parameter λ) is introduced to ensure the strong convexity of the inner-level attack objective within the constraint set $\boldsymbol{\delta} \in \mathcal{C}$ (the closed-form solution of the lower-level solution is given by (6)). Note that imposing such a strongly convex regularizer is also commonly used to stabilize the convergence of min-max optimization and BLO [43, 38]. If we set $\mathbf{z} = \boldsymbol{\delta}_0$ and $\lambda = 1/\alpha$, then (6) precisely depicts the inner maximization step used in FAST-AT.

– Second, by substituting (6) into the upper-level problem of (5), we can then use (4) to compute the stochastic gradients of the upper-level problem. If the stochastic gradient can be precisely computed, then we can update the model parameters $\boldsymbol{\theta}$ using SGD based on (4). That is, $\boldsymbol{\theta} \leftarrow \boldsymbol{\theta} - \beta \frac{d\ell_{\text{tr}}(\boldsymbol{\theta}_t, \boldsymbol{\delta}^*(\boldsymbol{\theta}))}{d\boldsymbol{\theta}}$ (with learning rate β). However, generally speaking, the IG function $\frac{d\boldsymbol{\delta}^*(\boldsymbol{\theta})^\top}{d\boldsymbol{\theta}}$ involved in (4) may not be differentiable, and even it is, the computation may not be easy. For our case, $\boldsymbol{\delta}^*(\boldsymbol{\theta})$ expressed in (6) involves both a projection operator and a sign operation, which can be particularly difficult to compute. To proceed, let us make the following approximations. We assume that the chain rule of the derivative of $\boldsymbol{\delta}^*(\boldsymbol{\theta})$ holds w.r.t. $\boldsymbol{\theta}$, implying the differentiability of the projection operation and the sign operation. Then, based on the closed-form of $\boldsymbol{\delta}^*(\boldsymbol{\theta})$ in (6), IG is approximately equal to

$$\frac{d\boldsymbol{\delta}^*(\boldsymbol{\theta})^\top}{d\boldsymbol{\theta}} = \mathbf{0}, \quad (7)$$

where we use two facts: (1) The linearization point \mathbf{z} is independent of $\boldsymbol{\theta}$, i.e. $\mathbf{z} = \boldsymbol{\delta}_0$; And (2) $\frac{d\text{sign}(\cdot)}{d\boldsymbol{\theta}} = \mathbf{0}$ holds almost everywhere. Clearly, the use of gradient sign method simplifies the IG computation. Substituting (7) into (4), the upper-level gradient is approximated by $\frac{d\ell_{\text{tr}}(\boldsymbol{\theta}, \boldsymbol{\delta}^*(\boldsymbol{\theta}))}{d\boldsymbol{\theta}} \approx \nabla_{\boldsymbol{\theta}}\ell_{\text{tr}}(\boldsymbol{\theta}, \boldsymbol{\delta}^*(\boldsymbol{\theta})) := \tilde{\mathbf{h}}(\boldsymbol{\theta})$, and the upper-level optimization of problem (5) becomes $\boldsymbol{\theta} \leftarrow \boldsymbol{\theta} - \beta \tilde{\mathbf{h}}(\boldsymbol{\theta})$, which is the same as the outer minimization step used in

FAST-AT. In a nutshell, the BLO solver of problem (5), which calls the IG computation based on (6), eventually reduces to the FAST-AT algorithm.

The aforementioned analysis shows that FAST-AT can be viewed as using an approximated stochastic gradient algorithm to solve the linearized BLO (5), with the linearization point \mathbf{z} and the regularization parameter λ set as $\mathbf{z} = \delta_0$ and $\lambda = 1/\alpha$. However, since a series of approximations have been used when arriving at the approximated gradient $\tilde{\mathbf{h}}(\boldsymbol{\theta})$ used by FAST-AT, it is no longer clear if the resulting algorithm can still sufficiently reduce the objective function of the upper-level problem. Additionally, based on the fact that the lower-level problem of (5) involves the discrete sign operator, it is unlikely (if not impossible) that any approximated stochastic gradient based algorithms developed for it can possess any strong theoretical guarantees.

4 FAST-BAT: Advancing FAST-AT by BLO

FAST-BAT and rationale. The key take-away from (5) is that the conventional FAST-AT adopts the *sign of input gradient* to linearize the lower-level attack objective. However, a more natural choice is to use the first-order Taylor expansion for linearization. By doing so, problem (5) can be modified to the following form:

$$\begin{aligned} & \underset{\boldsymbol{\theta}}{\text{minimize}} && \mathbb{E}_{(\mathbf{x}, y) \in \mathcal{D}}[\ell_{\text{tr}}(\boldsymbol{\theta}, \boldsymbol{\delta}^*(\boldsymbol{\theta}))] \\ & \text{subject to} && \boldsymbol{\delta}^*(\boldsymbol{\theta}) = \arg \min_{\boldsymbol{\delta} \in \mathcal{C}} [(\boldsymbol{\delta} - \mathbf{z})^\top \nabla_{\boldsymbol{\delta}=\mathbf{z}} \ell_{\text{atk}}(\boldsymbol{\theta}, \boldsymbol{\delta}) + (\lambda/2) \|\boldsymbol{\delta} - \mathbf{z}\|_2^2]. \end{aligned} \quad (8)$$

Similar to (6), the lower-level problem can be solved analytically as

$$\boldsymbol{\delta}^*(\boldsymbol{\theta}) = \mathcal{P}_{\mathcal{C}}(\mathbf{z} - (1/\lambda) \nabla_{\boldsymbol{\delta}=\mathbf{z}} \ell_{\text{atk}}(\boldsymbol{\theta}, \boldsymbol{\delta})). \quad (9)$$

In contrast to (7), the IG associated with (8) cannot be approximated by zeros since the gradient sign operation is not present in (9). To compute IG, the auto-differentiation (which calls the chain rule) can be applied to the closed-form of $\boldsymbol{\delta}^*(\boldsymbol{\theta})$. However, this will not give us an accurate and generalizable IG solution since the projection operation $\mathcal{P}_{\mathcal{C}}$ is *not* smooth everywhere and thus, the use of chain rule does not yield a rigorous derivation. In the following subsection, we address the *IG challenge* in a theoretically-grounded manner.

IG theory for FAST-BAT. The problem of FAST-BAT (8) falls into a class of very challenging BLO problems, which requires *constrained* lower-level optimization. The unconstrained case is easier to handle since one can apply the implicit function theory to the stationary condition of the lower-level problem to obtain IG [38]. Yet, in the case of *constrained* problems, a stationary point could violate the constraints, and thus the stationary condition becomes non-applicable.

Fortunately, in problem (8), we are dealing with a special class of lower-level constraints – *linear constraints*. Let us rewrite the constraints below:

$$\|\boldsymbol{\delta}\|_{\infty} \leq \epsilon, \boldsymbol{\delta} \in [-\mathbf{x}, \mathbf{1} - \mathbf{x}] \iff \mathbf{B}\boldsymbol{\delta} \leq \mathbf{b}, \text{ with } \mathbf{B} := \begin{bmatrix} \mathbf{I} \\ -\mathbf{I} \end{bmatrix}, \mathbf{b} := \begin{bmatrix} \min\{\epsilon\mathbf{1}, \mathbf{1} - \mathbf{x}\} \\ -\max\{-\epsilon\mathbf{1}, -\mathbf{x}\} \end{bmatrix}. \quad (10)$$

By exploiting above linearly constrained problem structure, we show that the IG challenge associated with (8) can be addressed via *Karush–Kuhn–Tucker (KKT)* conditions. We summarize our main theoretical results (Proposition 1 and Corollary 1) below and refer readers to Appendix A for detailed derivation.

Proposition 1 *For the BLO problem (8), let $g(\boldsymbol{\theta}, \boldsymbol{\delta}^*)$ denote its lower-level objective function evaluated at $\boldsymbol{\delta}^*$ given $\boldsymbol{\theta}$, then the analytical form of IG (implicit gradient) is given by*

$$\begin{aligned} \frac{d\boldsymbol{\delta}^*(\boldsymbol{\theta})^\top}{d\boldsymbol{\theta}} &= -\nabla_{\boldsymbol{\theta}\boldsymbol{\delta}} g(\boldsymbol{\theta}, \boldsymbol{\delta}^*) \nabla_{\boldsymbol{\delta}\boldsymbol{\delta}} g(\boldsymbol{\theta}, \boldsymbol{\delta}^*)^{-1} \\ &\quad + \nabla_{\boldsymbol{\theta}\boldsymbol{\delta}} g(\boldsymbol{\theta}, \boldsymbol{\delta}^*) \nabla_{\boldsymbol{\delta}\boldsymbol{\delta}} g(\boldsymbol{\theta}, \boldsymbol{\delta}^*)^{-1} \mathbf{B}_0^\top [\mathbf{B}_0 \nabla_{\boldsymbol{\delta}\boldsymbol{\delta}} g(\boldsymbol{\theta}, \boldsymbol{\delta}^*)^{-1} \mathbf{B}_0^\top]^{-1} \mathbf{B}_0 \nabla_{\boldsymbol{\delta}\boldsymbol{\delta}} g(\boldsymbol{\theta}, \boldsymbol{\delta}^*)^{-1}, \end{aligned} \quad (11)$$

where $\boldsymbol{\delta}^*$ is given by (9) (the dependence on $\boldsymbol{\theta}$ is omitted for ease of notation), $\nabla_{\boldsymbol{\theta}\boldsymbol{\delta}} g(\boldsymbol{\theta}, \boldsymbol{\delta}^*) \in \mathbb{R}^{n \times d}$ denotes the second-order partial derivatives evaluated at $(\boldsymbol{\theta}, \boldsymbol{\delta}^*)$, and \mathbf{B}_0 denotes the sub-matrix of \mathbf{B} that only corresponds to the active constraints at $\boldsymbol{\delta}^*$, i.e., those in $\mathbf{B}\boldsymbol{\delta}^* \leq \mathbf{b}$ satisfied with the equality.

It is clear from (11) that the computation of IG requires the second-order derivatives as well as matrix inversion. This is computationally intensive. Recall from (8) that the Hessian matrix $\nabla_{\boldsymbol{\delta}\boldsymbol{\delta}} g$ of the lower-level

objective function is given by $\nabla_{\delta\delta}g(\boldsymbol{\theta}, \boldsymbol{\delta}^*) = \nabla_{\delta\delta}\ell_{\text{atk}} + \lambda\mathbf{I}$. This inspires us to impose the Hessian-free approximation, *i.e.*, $\nabla_{\delta\delta}\ell_{\text{atk}} = \mathbf{0}$. The rationale behind the Hessian-free assumption is that ReLU-based neural networks commonly lead to a piece-wise linear decision boundary w.r.t. the inputs [44, 45], and thus, its second-order derivative (Hessian) $\nabla_{\delta\delta}\ell_{\text{atk}}$ is close to zero. Furthermore, in Section 5.2 we will empirically show that the Hessian-free assumption is reasonable for both ReLU and non-ReLU neural networks. In a nutshell, we approximate the Hessian matrix by

$$\nabla_{\delta\delta}g(\boldsymbol{\theta}, \boldsymbol{\delta}^*(\boldsymbol{\theta})) = \nabla_{\delta\delta}\ell_{\text{atk}} + \lambda\mathbf{I} = \mathbf{0} + \lambda\mathbf{I}. \quad (12)$$

With the aid of (12), we can achieve a simplified closed-form of IG; see Corollary 1.

Corollary 1 *With a Hessian-free assumption, *i.e.*, $\nabla_{\delta\delta}\ell_{\text{atk}} = \mathbf{0}$, the IG (implicit gradient) of (8) is*

$$\frac{d\boldsymbol{\delta}^*(\boldsymbol{\theta})^\top}{d\boldsymbol{\theta}} = -(1/\lambda)\nabla_{\boldsymbol{\theta}\delta}\ell_{\text{atk}}(\boldsymbol{\theta}, \boldsymbol{\delta}^*)\mathbf{H}_C, \text{ with } \mathbf{H}_C := [1_{p_1 < \delta_1^* < q_1} \mathbf{e}_1 \quad \cdots \quad 1_{p_d < \delta_d^* < q_d} \mathbf{e}_d]. \quad (13)$$

In $\mathbf{H}_C \in \mathbb{R}^{d \times d}$, $1_{p_i < \delta_i^* < q_i} \in \{0, 1\}$ denotes the indicator function over the constraint of $\{\delta_i \mid p_i < \delta_i^* < q_i\}$, which returns 1 if the constraint is satisfied, δ_i^* denotes the i th entry of $\boldsymbol{\delta}^*(\boldsymbol{\theta})$, $p_i = \max\{-\epsilon, -x_i\}$ and $q_i = \min\{\epsilon, 1 - x_i\}$ characterize the boundary of the linear constraint (10) for the variable δ_i , and $\mathbf{e}_i \in \mathbb{R}^d$ denotes the basis vector with the i th entry being 1 and others being 0s.

FAST-BAT algorithm and implementation. Similar to FAST-AT or AT, the FAST-BAT algorithm also follows the principle of alternating optimization. Specifically, it consists of the IG-based upper-level gradient descent (4), interlaced with the lower-level optimal attack (9). We summarize the FAST-BAT algorithm below.

FAST-BAT algorithm

The $(t + 1)$ th upper-level iteration of FAST-BAT is given below

- ① (*Lower-level solution*): Obtain $\boldsymbol{\delta}^*(\boldsymbol{\theta}_t)$ from (9);
- ② (*Upper-level model training*): Integrating the IG (13) into (4), call SGD to update

$$\boldsymbol{\theta}_{t+1} = \boldsymbol{\theta}_t - \alpha_1 \nabla_{\boldsymbol{\theta}} \ell_{\text{tr}}(\boldsymbol{\theta}_t, \boldsymbol{\delta}^*(\boldsymbol{\theta}_t)) - \alpha_2 (-1/\lambda) \nabla_{\boldsymbol{\theta}\delta} \ell_{\text{atk}}(\boldsymbol{\theta}_t, \boldsymbol{\delta}^*(\boldsymbol{\theta}_t)) \mathbf{H}_C \nabla_{\delta} \ell_{\text{tr}}(\boldsymbol{\theta}_t, \boldsymbol{\delta}^*(\boldsymbol{\theta}_t)), \quad (14)$$

where $\alpha_1, \alpha_2 > 0$ are learning rates associated with the standard model gradient and the IG-augmented descent direction, respectively.

It is clear from (14) that to train a robust model, FAST-BAT can be decomposed into the regular FAST-AT update (*i.e.*, the term multiplied by α_1) and the additional update that involves IG, (*i.e.*, the term multiplied by α_2). To successfully implement FAST-BAT, we highlight some key hyper-parameter setups that are different from FAST-AT [1] and FAST-AT-GA [18].

Remark 1 (Choice of learning rate for α_2 .) *In (14), if $\alpha_2 = 0$, then the update of the upper-level model parameter is independent of IG, similar the ordinary adversarial training recipe when updating model parameters. In Sec. 5.1, we will show that properly choosing α_2 plays a positive role in alleviating catastrophic robust overfitting. Meanwhile, λ in (8) could also affect the accuracy-robustness tradeoff. For example, if $\lambda \rightarrow \infty$, then $\boldsymbol{\delta} = \mathbf{0}$ (no robustness gain). Spurred by above, we choose the following combination of α_2 and λ , $\alpha_2/\lambda = 0.1\alpha_1$, which works well in practice; see Table A2.*

Remark 2 (Choice of linearization point \mathbf{z} .) *To specify (8), we investigate two classes of linearization schemes. The first class is random constant linearization, which includes: “uniformly random linearization”, *i.e.*, $\mathbf{z} = \boldsymbol{\delta}_0$ as FAST-AT, and “random corner linearization” under the ϵ -radius ℓ_∞ -ball, *i.e.*, $\mathbf{z} \in \{-\epsilon, \epsilon\}^d$. The second class is 1-step perturbation warm-up-based linearization, which includes the other two specifications: “1-step PGD” $\mathbf{z} = P_C(\boldsymbol{\delta}_0 + \alpha \cdot \text{sign}(\nabla_{\delta} \ell_{\text{tr}}(\boldsymbol{\theta}_t, \boldsymbol{\delta}_0)))$, and “1-step PGD w/o sign” $\mathbf{z} = P_C(\boldsymbol{\delta}_0 + \alpha \nabla_{\delta} \ell_{\text{tr}}(\boldsymbol{\theta}_t, \boldsymbol{\delta}_0))$. We consider the aforementioned linearization schemes as their computation complexities are less than or close to the complexity of one-step attack generation. As a result, FAST-BAT combined with these linearizations takes computation cost comparable to the baselines FAST-AT and FAST-AT-GA. In experiments, we find that FAST-BAT using “1-step PGD w/o sign” typically leads to the best defensive performance; see justification in Table A4. We follow this experiment setup in the sequel.*

5 Experiments

5.1 Experiment Setup

Datasets and model architectures. We will evaluate the effectiveness of our proposal under CIFAR-10 [46] and ImageNet [47]. Unless specified otherwise, we will train DNN models PreActResNet (PARN)-18 [48] for CIFAR-10, and ResNet (RN)-50 [49] for ImageNet. As a part of the ablation study, we also train larger models PARN-50 and WideResNet (WRN)-16-8 [50] on CIFAR-10. Our extensive empirical studies are primarily built on CIFAR-10 and some ImageNet results are reported in Appendix D. The code of our experiments is available at https://github.com/NormalUhr/Fast_BAT.git.

Baselines. We consider three methods as our baselines: FAST-AT [1], FAST-AT-GA [18], and PGD-2-AT [5], *i.e.*, the 2-step PGD attack-based AT. The primal criterion of baseline selection is computation complexity. The training time of all methods including ours falls between the time of FAST-AT and that of FAST-AT-GA.

Training details. We choose the training perturbation strength $\epsilon \in \{2, 4, \dots, 16\}/255$ for CIFAR-10 and $\epsilon = 2/255$ for ImageNet following [1, 18]. Throughout the experiments, we utilize an SGD optimizer with a momentum of 0.9 and weight decay of 5×10^{-4} . For CIFAR-10, we train each model for 20 epochs in total, where we use the cyclic scheduler to adjust the learning rate. The learning rate linearly ascends from 0 to 0.2 within the first 10 epochs and then reduces to 0 within the last 10 epochs. Our batch size is set to 128 for all settings. In the implementation of FAST-BAT, we adjust the hyperparameter λ from 255/5000 to 255/2000 based on the specification of train-time ϵ . For ImageNet, we strictly follow the setup given by [1] and we choose the train-time attack budget as $\epsilon = 2/255$. For each method, we use the early stopping method to pick the model with the best robust accuracy, following [21]. All the CIFAR-10 experiments are conducted on a single Tesla P-100 GPU and all ImageNet experiments run on a single machine with two Tesla P-100s. All the baselines are implemented using the recommended training configurations in their official GitHub repos. We refer readers to Appendix C for more details on the training setup.

Evaluation details. For adversarial evaluation, we report robust test accuracy (RA) of a learned model against PGD attacks [5] (**RA-PGD**). Unless otherwise specified, we set the test-time perturbation strength (ϵ) same as the train-time value, and take 50-step PGD with 10 restarts for both CIFAR-10 and ImageNet evaluation. Since AutoAttack [22] is known as the strongest robust benchmark evaluation metric (given as an ensemble attack), we also measure robust accuracy against AutoAttack, termed **RA-AA**. Further, we measure the standard accuracy (SA) against natural examples. Results are averaged over 5 independent trials with different seeds.

Table 2: SA, RA-PGD and RA-AA of different robust training methods in the setup (CIFAR-10, PARN-18 training with $\epsilon = 8/255$) and (CIFAR-10, PARN-18 training with $\epsilon = 16/255$), respectively. All the results are averaged over 5 independent trials with different random seeds.

CIFAR-10, PARN-18 trained with $\epsilon = 8/255$								
Method	SA (%)	RA-PGD (%)				RA-AA (%)		
		$\epsilon = 4$	$\epsilon = 8$	$\epsilon = 12$	$\epsilon = 16$	$\epsilon = 2$	$\epsilon = 8$	$\epsilon = 16$
FAST-AT	81.89±0.31	65.92 ±0.11	45.44 ±0.38	23.69 ±0.34	9.56 ±0.26	72.54 ±0.20	41.95 ±0.13	7.91 ±0.06
FAST-AT-GA	79.78±0.47	65.74 ±0.19	47.32 ±0.35	28.67 ±0.26	11.57±0.32	71.60 ±0.39	43.45 ±0.27	9.48 ±0.15
PGD-2-AT	83.26 ±0.28	65.59 ±0.34	44.71 ±0.42	23.67 ±0.35	9.42 ±0.33	73.28 ±0.15	41.73 ±0.20	7.54±0.25
FAST-BAT	79.47 ±0.14	66.26 ±0.08	48.67 ±0.18	29.87 ±0.46	14.00 ±0.21	72.07 ±0.22	44.86 ±0.34	11.51 ±0.20
CIFAR-10, PARN-18 trained with $\epsilon = 16/255$								
FAST-AT	46.13±2.25	42.74 ±0.91	37.17 ±0.74	27.99 ±0.72	21.92 ±0.71	36.31 ±2.20	31.66 ±0.27	12.48 ±0.29
FAST-AT-GA	58.53 ±1.20	51.71 ±0.99	43.86 ±0.67	35.46 ±0.36	26.29 ±0.14	53.61 ±1.10	38.69 ±0.56	18.11 ±0.36
PGD-2-AT	69.40 ±0.30	59.25 ±0.16	48.79 ±0.31	32.12 ±0.63	24.30 ±0.46	61.90 ±0.28	41.59 ±0.22	15.40 ±0.29
FAST-BAT	67.81 ±0.18	59.35 ±0.13	49.05 ±0.12	37.71 ±0.36	26.07 ±0.28	62.16 ±0.14	43.64 ±0.26	18.18 ±0.34

5.2 Results

Overall performance of FAST-BAT. In Table 2 and A1, we compare the performance of our proposed FAST-BAT with baselines on CIFAR-10 and ImageNet, respectively.

First, we find that FAST-BAT consistently outperforms the other baselines across datasets and attack types. For example, FAST-BAT at least improves 1.35% RA-PGD and 1.41% RA-AA with test-time $\epsilon = 8/255$ in the training setup (CIFAR-10, $\epsilon = 8/255$). On ImageNet, FAST-BAT outperforms FAST-AT by 1.23% when facing attacks with $\epsilon = 2/255$.

Second, FAST-BAT leads to a better SA-RA trade-off compared with the other baselines. For example, in the setup of (CIFAR-10, PARN-18 trained with $\epsilon = 8/255$), we observe that FAST-BAT outperforms FAST-AT-GA in RA, without losing SA. And in the setup of (CIFAR-10, PARN-18 trained with $\epsilon = 16/255$), FAST-BAT significantly outperforms FAST-AT-GA, with 9.28% SA improvement and comparable or even better RA. Compared with PGD-2-AT, FAST-BAT is much more resilient against strong adversaries, e.g., $\epsilon = 16/255$.

Third, the robustness advantage of our method becomes more notable when the test-time attack budget becomes smaller than the train-time budget. For example, the RA-AA improvement of FAST-BAT over FAST-AT-GA grows from 0.07% (evaluated at $\epsilon = 16/255$) to 4.95% (evaluated at $\epsilon = 8/255$), and 8.55% (evaluated at $\epsilon = 2/255$) in the case of (CIFAR-10, trained with $\epsilon = 16/255$).

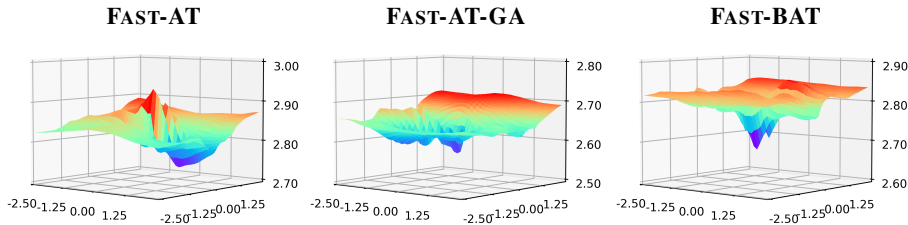


Figure 1: Visualization of adversarial loss landscapes of FAST-AT, FAST-AT-GA and FAST-BAT trained using the ResNet-18 model on the CIFAR-10 dataset. The losses are calculated w.r.t. the same image example ID #001456, and the landscape is obtained by tracking the loss changes w.r.t. input variations following [51]. That is, the loss landscape is generated by $z = \text{loss}(I + x \cdot \mathbf{r}_1 + y \cdot \mathbf{r}_2)$, where I denotes an image, and the x -axis and the y -axis correspond to linear coefficients associated with the sign-based attack direction $\mathbf{r}_1 = \text{sign}(\nabla_I \text{loss}(I)) \hat{\mathbf{x}}$ and a random direction $\mathbf{r}_2 \sim \text{Rademacher}(0.5)$, respectively.

Performance under different model architectures. Besides PARN-18 reported above, Table 3 presents results on both deeper (PARN-50) and wider (WRN-18-6) models. As we can see, FAST-BAT consistently yields RA improvement over the other baselines. We also note that PGD-2-AT could be a competitive baseline in terms of SA, e.g., the case of (PARN-50, $\epsilon = 8/255$). In contrast to FAST-AT and FAST-AT-GA, FAST-BAT is the only approach that yields an evident RA improvement over PGD-2-AT.

Table 3: Performance of different robust training methods under different model types. All the models are both trained and evaluated with the same perturbation strength ϵ .

Model	Method	SA(%) ($\epsilon = 8/255$)	RA-PGD(%) ($\epsilon = 8/255$)	SA(%) ($\epsilon = 16/255$)	RA-PGD(%) ($\epsilon = 16/255$)
PARN-50	FAST-AT	73.15±6.10	41.03±2.99	43.86±4.31	22.08±0.27
	FAST-AT-GA	77.40±0.81	46.16±0.98	42.28±6.69	22.87±1.25
	PGD-2-AT	83.53±0.17	46.17±0.59	68.88±0.39	22.37±0.41
	FAST-BAT	78.91±0.68	49.18±0.35	69.01±0.19	24.55±0.06
WRN-16-8	FAST-AT	84.39±0.46	45.80±0.57	49.39±2.17	21.99±0.41
	FAST-AT-GA	81.51±0.38	48.29±0.20	45.95±13.65	23.10±3.90
	PGD-2-AT	85.52±0.14	45.47±0.14	72.11±0.33	23.61±0.16
	FAST-BAT	81.66±0.54	49.93±0.36	68.12±0.47	25.63±0.44

Mitigation of robustness catastrophic overfitting. As shown in [18], FAST-AT suffers robustness catastrophic overfitting when the train-time and test-time attack strength ϵ grows. Following [18], Figure 2 presents

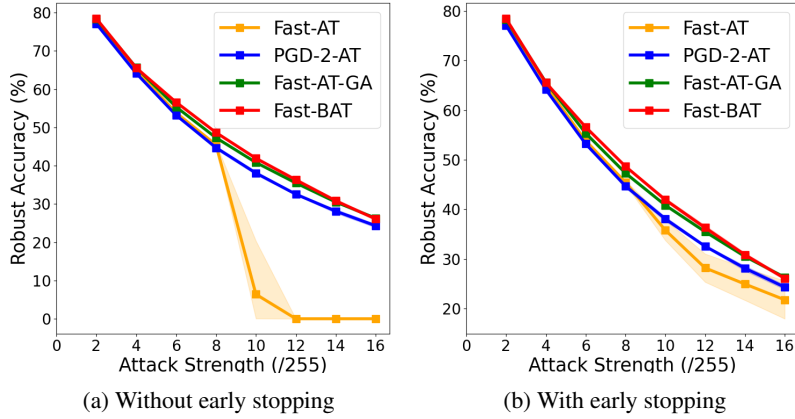


Figure 2: RA-PGD of different robust training methods for (CIFAR-10, PARN-18) with the same training and evaluation attack strengths.

two RA-PGD trajectories, *i.e.*, training w/o early stopping and training w/ early stopping, versus the train- and test-time ϵ . As we can see, FAST-AT encounters a sharp RA drop when $\epsilon > 8$ when early stopping is not used, consistent with [18]. Assisted by early stopping, the overfitting of RA can be alleviated to some extent for FAST-AT, but its performance still remains the worst. Moreover, different from [18], we find that PGD-2-AT yields resilient performance against robustness catastrophic overfitting. Our implementation gives a more positive baseline than the implementation of PGD-2-AT in [18], since the latter did not use random initialization to generate train-time attacks. Furthermore, Figure 2 shows that our proposal mitigates the issue of robustness catastrophic overfitting and yields improved RA over the other baselines. We highlight that such an achievement made by FAST-BAT is ‘free’ of any robustness stability regularization, like gradient alignment used in FAST-AT-GA.

Gradient alignment for ‘free’. As shown by [18], the phenomenon of *catastrophic overfitting* occurs with the local non-linearity of deep networks, which can be measured by the gradient alignment (GA) score $\mathbb{E}_{(\mathbf{x}, y) \sim \mathcal{D}, \boldsymbol{\eta} \sim \mathcal{U}([- \epsilon, \epsilon]^d)} [\cos(\nabla_{\mathbf{x}} \ell_{\text{tr}}(\mathbf{x}, y; \boldsymbol{\theta}), \nabla_{\mathbf{x}} \ell_{\text{tr}}(\mathbf{x} + \boldsymbol{\eta}, y; \boldsymbol{\theta}))]$, where \mathcal{U} denotes the randomly uniform distribution. GA is a key performance indicator to measure the appearance of robustness catastrophic overfitting, as catastrophic overfitting is always accompanied with a sharp GA drop in the training trajectory of the robustly trained model. In our paper, we calculate the GA for each method on the test set at the end of each epoch throughout the training process in Figure 3. The insight from Figure 2 suggested that FAST-BAT can mitigate overfitting without using explicit GA regularization. Spurred by above, Figure 3 presents the GA score versus the training epoch number, where GA characterizes the sensitivity of loss landscape against random input perturbations; see derivations in [18]. The higher GA is, the more stable the robust training is. Figure 3 shows that FAST-BAT automatically enforces GA and it outperforms FAST-AT and PGD-2-AT. FAST-BAT remains very close to FAST-AT-GA, which maximizes GA using an extra train-time regularization. The above empirical results imply that gradient alignment may just be a necessary condition for avoiding catastrophic overfitting, but not a sufficient one. A possible justification can be made from the perspective of the flatness of the loss landscape. A higher gradient alignment implies a flatter loss landscape with respect to input perturbations. However, the direct penalization on the norm of the input gradient may not achieve the state-of-the-art model robustness.

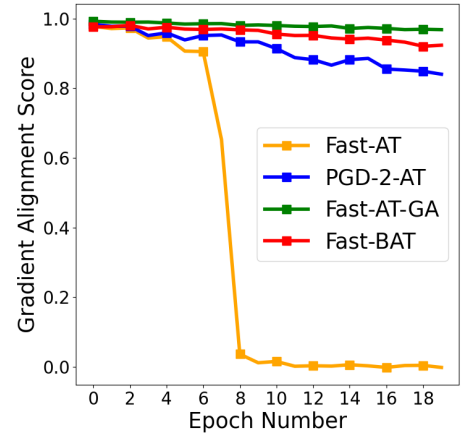


Figure 3: The training trajectory of GA score over different training methods.

Sanity check for obfuscated gradients As pointed out by [9], model robustness could be overestimated due to obfuscated gradients. The model with obfuscated gradients could have ‘obfuscated’ stronger resilience to white-box attacks than transfer (black-box) attacks. To justify the validity of FAST-BAT, Table 4 summarizes the comparison between our proposal and the other baselines when facing white-box adaptive and black-box transfer attacks. Firstly, RA increases if the transfer attack is present for each method, implying that the transfer attack is

Table 4: RA of robust PARN-18 trained by the four different methods against adaptive attacks (‘RA-PGD’ column) and transfer attacks (‘Transfer Attack’ columns). Naturally trained PARN-18, PARN-50, and WRN-16-8 are used as surrogate models for PGD-20 attack with $\epsilon = 8/255$.

Method	RA-PGD(%)	RA-Transfer Attack(%)		
		PARN-18	PARN-50	WRN-16-8
FAST-AT	45.44±0.06	76.35±0.12	76.94±0.14	77.23±0.21
PGD-2-AT	44.71±0.04	77.56±0.14	78.64±0.12	78.84±0.17
FAST-AT-GA	47.31±0.05	77.34±0.13	78.34±0.13	78.53±0.12
FAST-BAT(Ours)	48.67±0.05	78.03 ±0.15	79.93 ±0.12	79.21 ±0.15

Table 5: Performance of Hessian-free and Hessian-aware FAST-BAT on CIFAR-10. We train and evaluate with the same attack budgets $\epsilon = 8/255$ and $\epsilon = 16/255$ to show the influence brought by Hessian matrix.

Method	RA-PGD (%)	RA-PGD (%)	RA-AA (%)	RA-AA (%)	SA (%)	SA (%)	Time (s/epoch)
	($\epsilon = 8/255$)	($\epsilon = 16/255$)	($\epsilon = 8/255$)	($\epsilon = 16/255$)	($\epsilon = 8/255$)	($\epsilon = 16/255$)	
Hessian-free Fast-BAT	48.67	26.07	44.86	18.18	79.47	67.81	135
Hessian-aware Fast-BAT	48.52	26.12	44.81	18.31	79.54	67.93	179

weaker than the white-box adaptive attack. This is desired in the absence of obfuscated gradients. Moreover, FAST-BAT consistently outperforms the other three baselines when defending against both adaptive and transfer attacks. The absence of obfuscated gradients can also be justified by RA vs. the growth of the attack budget ϵ in Table 2, and the flatness of adversarial loss landscape in Figure. 1.

The validity of the Hessian-free assumption on ReLU-based neural networks. In Corollary 1, the Hessian-free assumption, *i.e.* $\nabla_{\delta\delta}\ell_{\text{atk}} = 0$, was made to simplify the computation of IG term (implicit gradient). To examine how the Hessian matrix $\nabla_{\delta\delta}\ell_{\text{atk}}$ affects the performance of Fast-BAT, we conduct experiments to compare the Hessian-free FAST-BAT with the Hessian-aware version. In Hessian-aware FAST-BAT, the implicit gradient is calculated based on (24). In Table 5, the results do not indicate much difference when Hessian is used. However, the extra computations required to evaluate the Hessian heavily slows down FAST-BAT as around 30% more time is needed. Therefore, the Hessian-free assumption is reasonable and also necessary in terms of the efficiency of the algorithm.

The validity of the Hessian-free assumption on non-ReLU based neural networks. The Hessian-free assumption is based on the fact that the commonly used ReLU activation function is piece-wise linear *w.r.t.* input. We further conduct experiments to verify the feasibility of such an assumption on models with non-ReLU activation functions. We choose two commonly used activation functions, Swish [52] and Softplus, as alternatives for the non-smooth ReLU function. We compare the results both calculating Hessian as well as the Hessian-free version to see if the Hessian-free assumption still holds for the non-ReLU neural network. The results are shown in Table 6. As we can see, the use of Hessian does not affect performance much. A similar phenomenon can be observed across different ϵ and different model activation functions (ReLU, Softplus, and Swish). However, the introduction of Hessian leads to an increase in time consumption by more than 30%. Therefore, we can draw the conclusion that the Hessian-free assumption is reasonable across different activation function choices.

Ablation studies. In Appendix D, we present additional empirical studies including 1) the sensitivity analysis of the linearization hyperparameter λ , 2) the choice of the linearization point, and 3) the sensitivity analysis of α_2 .

6 Conclusion

In this paper, we introduce a novel bi-level optimization (BLO)-based fast adversarial training framework, termed FAST-BAT. The rationale behind designing fast robust training through the lens of BLO lies in two aspects. First, from the perspective of implicit gradients, we show that the existing FAST-AT framework is equivalent to the lower-level linearized BLO along the sign direction of the input gradient. Second, we show that FAST-BAT enables the least restriction to achieve improved stability of performance, mitigated catastrophic overfitting, and

Table 6: Performance of FAST-AT and FAST-BAT with different activation functions on CIFAR-10. ReLU, Swish and Softplus are taken into consideration. For FAST-BAT, we compare the Hessian-free and Hessian-aware version to verify the influence of Hessian matrix. The results are averaged over 3 independent trials.

Setting	SA (%)	RA-PGD (%)	SA (%)	RA-PGD (%)	Time (s/epoch)
	($\epsilon = 8/255$)	($\epsilon = 8/255$)	($\epsilon = 16/255$)	($\epsilon = 16/255$)	
Fast-AT-ReLU	81.88	45.44	46.13	21.75	42
Fast-BAT-ReLU (Hessian-aware)	79.54	48.52	67.93	26.12	179
Fast-BAT-ReLU (Hessian-free)	79.47	48.67	67.81	26.07	135
Fast-AT-Softplus	81.29	47.26	45.39	22.40	42
Fast-BAT-Softplus (Hessian-aware)	79.59	49.74	68.63	25.54	178
Fast-BAT-Softplus (Hessian-free)	79.48	49.67	68.57	25.59	137
Fast-AT-Swish	75.61	44.43	52.03	23.08	49
Fast-BAT-Swish (Hessian-aware)	73.93	45.97	62.49	23.99	196
Fast-BAT-Swish (Hessian-free)	73.89	45.90	62.59	23.81	141

enhanced accuracy-robustness trade-off. To the best of our knowledge, we for the first time establish the theory and the algorithmic foundation of BLO for adversarially robust training. Extensive experiments are provided to demonstrate the superiority of our method to state-of-the-art accelerated AT baselines. In the future, we plan to establish the convergence rate analysis of FAST-BAT.

References

- [1] Eric Wong, Leslie Rice, and J. Zico Kolter, “Fast is better than free: Revisiting adversarial training,” in *International Conference on Learning Representations*, 2020.
- [2] Ian J Goodfellow, Jonathon Shlens, and Christian Szegedy, “Explaining and harnessing adversarial examples,” *arXiv preprint arXiv:1412.6572*, 2014.
- [3] Nicholas Carlini and David Wagner, “Towards evaluating the robustness of neural networks,” in *IEEE Symposium on S&P*, 2017.
- [4] Nicolas Papernot, Patrick McDaniel, Somesh Jha, Matt Fredrikson, Z Berkay Celik, and Ananthram Swami, “The limitations of deep learning in adversarial settings,” in *Security and Privacy (EuroS&P), 2016 IEEE European Symposium on*. IEEE, 2016, pp. 372–387.
- [5] Aleksander Madry, Aleksandar Makelov, Ludwig Schmidt, Dimitris Tsipras, and Adrian Vladu, “Towards deep learning models resistant to adversarial attacks,” in *International Conference on Learning Representations*, 2018.
- [6] Hongyang Zhang, Yaodong Yu, Jiantao Jiao, Eric P Xing, Laurent El Ghaoui, and Michael I Jordan, “Theoretically principled trade-off between robustness and accuracy,” *ICML*, 2019.
- [7] Ali Shafahi, Mahyar Najibi, Mohammad Amin Ghiasi, Zheng Xu, John Dickerson, Christoph Studer, Larry S Davis, Gavin Taylor, and Tom Goldstein, “Adversarial training for free!,” in *Advances in Neural Information Processing Systems*, 2019, pp. 3353–3364.
- [8] Dinghui Zhang, Tianyuan Zhang, Yiping Lu, Zhanxing Zhu, and Bin Dong, “You only propagate once: Accelerating adversarial training via maximal principle,” *arXiv preprint arXiv:1905.00877*, 2019.
- [9] Anish Athalye, Nicholas Carlini, and David Wagner, “Obfuscated gradients give a false sense of security: Circumventing defenses to adversarial examples,” *arXiv preprint arXiv:1802.00420*, 2018.
- [10] Christian Szegedy, Wojciech Zaremba, Ilya Sutskever, Joan Bruna, Dumitru Erhan, Ian Goodfellow, and Rob Fergus, “Intriguing properties of neural networks,” *International Conference on Learning Representations*, 2014.
- [11] Alexey Kurakin, Ian J. Goodfellow, and Samy Bengio, “Adversarial machine learning at scale,” *2017 ICLR*, vol. arXiv preprint arXiv:1611.01236, 2017.
- [12] Haichao Zhang and Jianyu Wang, “Towards adversarially robust object detection,” in *Proceedings of the IEEE/CVF International Conference on Computer Vision*, 2019, pp. 421–430.
- [13] Takeru Miyato, Andrew M Dai, and Ian Goodfellow, “Adversarial training methods for semi-supervised text classification,” *arXiv preprint arXiv:1605.07725*, 2016.
- [14] Chen Zhu, Yu Cheng, Zhe Gan, Siqi Sun, Tom Goldstein, and Jingjing Liu, “Freelb: Enhanced adversarial training for natural language understanding,” *arXiv preprint arXiv:1909.11764*, 2019.
- [15] Samuel G Finlayson, John D Bowers, Joichi Ito, Jonathan L Zittrain, Andrew L Beam, and Isaac S Kohane, “Adversarial attacks on medical machine learning,” *Science*, vol. 363, no. 6433, pp. 1287–1289, 2019.
- [16] Faisal Mahmood, Daniel Borders, Richard J Chen, Gregory N McKay, Kevan J Salimian, Alexander Baras, and Nicholas J Durr, “Deep adversarial training for multi-organ nuclei segmentation in histopathology images,” *IEEE transactions on medical imaging*, vol. 39, no. 11, pp. 3257–3267, 2019.
- [17] Cihang Xie, Yuxin Wu, Laurens van der Maaten, Alan L Yuille, and Kaiming He, “Feature denoising for improving adversarial robustness,” in *Proceedings of the IEEE/CVF Conference on Computer Vision and Pattern Recognition*, 2019, pp. 501–509.

- [18] Maksym Andriushchenko and Nicolas Flammarion, “Understanding and improving fast adversarial training,” in *NeurIPS*, 2020.
- [19] Bai Li, Shiqi Wang, Suman Jana, and Lawrence Carin, “Towards understanding fast adversarial training,” *arXiv preprint arXiv:2006.03089*, 2020.
- [20] Stephan Dempe, *Foundations of bilevel programming*, Springer Science & Business Media, 2002.
- [21] Leslie Rice, Eric Wong, and Zico Kolter, “Overfitting in adversarially robust deep learning,” in *International Conference on Machine Learning*. PMLR, 2020, pp. 8093–8104.
- [22] Francesco Croce and Matthias Hein, “Reliable evaluation of adversarial robustness with an ensemble of diverse parameter-free attacks,” in *International Conference on Machine Learning*. PMLR, 2020, pp. 2206–2216.
- [23] Kaidi Xu, Sijia Liu, Pu Zhao, Pin-Yu Chen, Huan Zhang, Quanfu Fan, Deniz Erdogmus, Yanzhi Wang, and Xue Lin, “Structured adversarial attack: Towards general implementation and better interpretability,” in *ICLR*, 2019.
- [24] Anish Athalye, Logan Engstrom, Andrew Ilyas, and Kevin Kwok, “Synthesizing robust adversarial examples,” in *International Conference on Machine Learning*, 2018, pp. 284–293.
- [25] Yao Deng, Xi Zheng, Tianyi Zhang, Chen Chen, Guannan Lou, and Miryung Kim, “An analysis of adversarial attacks and defenses on autonomous driving models,” in *2020 IEEE International Conference on Pervasive Computing and Communications (PerCom)*. IEEE, 2020, pp. 1–10.
- [26] K Naveen Kumar, C Vishnu, Reshmi Mitra, and C Krishna Mohan, “Black-box adversarial attacks in autonomous vehicle technology,” in *2020 IEEE Applied Imagery Pattern Recognition Workshop (AIPR)*. IEEE, 2020, pp. 1–7.
- [27] Simen Thys, Wiebe Van Ranst, and Toon Goedemé, “Fooling automated surveillance cameras: adversarial patches to attack person detection,” in *Proceedings of the IEEE Conference on Computer Vision and Pattern Recognition Workshops*, 2019, pp. 0–0.
- [28] Kaidi Xu, Gaoyuan Zhang, S. Liu, Quanfu Fan, Mengshu Sun, Hongge Chen, Pin-Yu Chen, Yanzhi Wang, and Xue Lin, “Adversarial T-Shirt! evading person detectors in a physical world,” in *ECCV*, 2020.
- [29] Yair Carmon, Aditi Raghunathan, Ludwig Schmidt, Percy Liang, and John C Duchi, “Unlabeled data improves adversarial robustness,” *arXiv preprint arXiv:1905.13736*, 2019.
- [30] T. Chen, S. Liu, S. Chang, Y. Cheng, L. Amini, and Z. Wang, “Adversarial robustness: From self-supervised pretraining to fine-tuning,” in *CVPR*, 2020.
- [31] Hadi Salman, Greg Yang, Jerry Li, Pengchuan Zhang, Huan Zhang, Ilya Razenshteyn, and Sebastien Bubeck, “Provably robust deep learning via adversarially trained smoothed classifiers,” *arXiv preprint arXiv:1906.04584*, 2019.
- [32] Luis Vicente, Gilles Savard, and Joaquim Júdice, “Descent approaches for quadratic bilevel programming,” *Journal of Optimization Theory and Applications*, vol. 81, no. 2, pp. 379–399, 1994.
- [33] Douglas J White and G Anandalingam, “A penalty function approach for solving bi-level linear programs,” *Journal of Global Optimization*, vol. 3, no. 4, pp. 397–419, 1993.
- [34] Stephen Gould, Basura Fernando, Anoop Cherian, Peter Anderson, Rodrigo Santa Cruz, and Edison Guo, “On differentiating parameterized argmin and argmax problems with application to bi-level optimization,” *arXiv preprint arXiv:1607.05447*, 2016.
- [35] Saeed Ghadimi and Mengdi Wang, “Approximation methods for bilevel programming,” *arXiv preprint:1802.02246*, 2018.

- [36] Prashant Khanduri, Siliang Zeng, Mingyi Hong, Hoi To Wai, Zhaoran Wang, and Zhuoran Yang, “A near-optimal algorithm for stochastic bilevel optimization via double-momentum,” in *Thirty-Fifth Conference on Neural Information Processing Systems*, 2021.
- [37] Kaiyi Ji, Junjie Yang, and Yingbin Liang, “Bilevel optimization: Nonasymptotic analysis and faster algorithms,” *arXiv preprint arXiv:2010.07962*, 2020.
- [38] Mingyi Hong, Hoi-To Wai, Zhaoran Wang, and Zhuoran Yang, “A two-timescale framework for bilevel optimization: Complexity analysis and application to actor-critic,” *arXiv preprint arXiv:2007.05170*, 2020.
- [39] Aravind Rajeswaran, Chelsea Finn, Sham Kakade, and Sergey Levine, “Meta-learning with implicit gradients,” *arXiv preprint arXiv:1909.04630*, 2019.
- [40] W Ronny Huang, Jonas Geiping, Liam Fowl, Gavin Taylor, and Tom Goldstein, “Metapoisson: Practical general-purpose clean-label data poisoning,” *arXiv preprint arXiv:2004.00225*, 2020.
- [41] Zhangyu Chen, Dong Liu, Xiaofei Wu, and Xiaochun Xu, “Research on distributed renewable energy transaction decision-making based on multi-agent bilevel cooperative reinforcement learning,” 2019.
- [42] Meisam Razaviyayn, Tianjian Huang, Songtao Lu, Maher Nouiehed, Maziar Sanjabi, and Mingyi Hong, “Nonconvex min-max optimization: Applications, challenges, and recent theoretical advances,” *IEEE Signal Processing Magazine*, vol. 37, no. 5, pp. 55–66, 2020.
- [43] Qi Qian, Shenghuo Zhu, Jiasheng Tang, Rong Jin, Baigui Sun, and Hao Li, “Robust optimization over multiple domains,” in *Proceedings of the AAAI Conference on Artificial Intelligence*, 2019, vol. 33, pp. 4739–4746.
- [44] Seyed-Mohsen Moosavi-Dezfooli, Alhussein Fawzi, Jonathan Uesato, and Pascal Frossard, “Robustness via curvature regularization, and vice versa,” in *Proceedings of the IEEE Conference on Computer Vision and Pattern Recognition*, 2019, pp. 9078–9086.
- [45] Motasem Alfarra, Adel Bibi, Hasan Hammoud, Mohamed Gaafar, and Bernard Ghanem, “On the decision boundaries of deep neural networks: A tropical geometry perspective,” *arXiv preprint arXiv:2002.08838*, 2020.
- [46] A. Krizhevsky and G. Hinton, “Learning multiple layers of features from tiny images,” *Master’s thesis, Department of Computer Science, University of Toronto*, 2009.
- [47] Jia Deng, Wei Dong, Richard Socher, Li-Jia Li, Kai Li, and Li Fei-Fei, “Imagenet: A large-scale hierarchical image database,” in *Computer Vision and Pattern Recognition, 2009. CVPR 2009. IEEE Conference on*. IEEE, 2009, pp. 248–255.
- [48] Kaiming He, Xiangyu Zhang, Shaoqing Ren, and Jian Sun, “Identity mappings in deep residual networks,” in *European conference on computer vision*. Springer, 2016, pp. 630–645.
- [49] Kaiming He, Xiangyu Zhang, Shaoqing Ren, and Jian Sun, “Deep residual learning for image recognition,” in *Proceedings of the IEEE conference on computer vision and pattern recognition*, 2016, pp. 770–778.
- [50] Sergey Zagoruyko and Nikos Komodakis, “Wide residual networks,” *arXiv preprint arXiv:1605.07146*, 2016.
- [51] Logan Engstrom, Andrew Ilyas, and Anish Athalye, “Evaluating and understanding the robustness of adversarial logit pairing,” *arXiv preprint arXiv:1807.10272*, 2018.
- [52] Prajit Ramachandran, Barret Zoph, and Quoc V Le, “Searching for activation functions,” *arXiv preprint arXiv:1710.05941*, 2017.

A Proof of Proposition 1 and Corollary 1

Proof: Upon defining $g(\boldsymbol{\theta}, \boldsymbol{\delta}) = (\boldsymbol{\delta} - \mathbf{z})^\top \nabla_{\boldsymbol{\delta}=\mathbf{z}} \ell_{\text{atk}}(\boldsymbol{\theta}, \boldsymbol{\delta}) + (\lambda/2) \|\boldsymbol{\delta} - \mathbf{z}\|_2^2$, we repeat (8) as

$$\begin{aligned} & \underset{\boldsymbol{\theta}}{\text{minimize}} && \mathbb{E}_{(\mathbf{x}, \mathbf{y}) \in \mathcal{D}} [\ell_{\text{tr}}(\boldsymbol{\theta}, \boldsymbol{\delta}^*(\boldsymbol{\theta}))] \\ & \text{subject to} && \boldsymbol{\delta}^*(\boldsymbol{\theta}) = \arg \min_{\mathbf{B}\boldsymbol{\delta} \leq \mathbf{b}} g(\boldsymbol{\theta}, \boldsymbol{\delta}), \end{aligned} \quad (15)$$

where we have used the expression of linear constraints in (10).

Our goal is to derive the IG $\frac{d\boldsymbol{\delta}^*(\boldsymbol{\theta})^\top}{d\boldsymbol{\theta}}$ shown in (4). To this end, we first build implicit functions by leveraging KKT conditions of the lower-level problem of (15). We say $\boldsymbol{\delta}^*(\boldsymbol{\theta})$ and $\boldsymbol{\lambda}^*(\boldsymbol{\theta})$ (Lagrangian multipliers) satisfy the KKT conditions:

$$\begin{aligned} \text{Stationarity:} & \quad \nabla_{\boldsymbol{\delta}} g(\boldsymbol{\theta}, \boldsymbol{\delta}^*(\boldsymbol{\theta})) + \mathbf{B}^\top \boldsymbol{\lambda}^*(\boldsymbol{\theta}) = \mathbf{0}, \\ \text{Complementary slackness:} & \quad \boldsymbol{\lambda}^*(\boldsymbol{\theta}) \cdot (\mathbf{B}\boldsymbol{\delta}^*(\boldsymbol{\theta}) - \mathbf{b}) = \mathbf{0} \\ \text{Dual feasibility:} & \quad \boldsymbol{\lambda}^*(\boldsymbol{\theta}) \geq \mathbf{0} \end{aligned} \quad (16)$$

where \cdot denotes the elementwise product.

Active constraints & definition of \mathbf{B}_0 : Let \mathbf{B}_0 denote the sub-matrix of \mathbf{B} and \mathbf{b}_0 the sub-vector of \mathbf{b} , which consists of only the *active constraints* at $\boldsymbol{\delta}^*(\boldsymbol{\theta})$, i.e., those satisfied with the equality $\mathbf{B}_0 \boldsymbol{\delta}^*(\boldsymbol{\theta}) = \mathbf{b}_0$ (corresponding to *nonzero* dual variables). The determination of active constraints is done given $\boldsymbol{\theta}$ at each iteration.

With the aid of $(\mathbf{B}_0, \mathbf{b}_0)$, KKT (16) becomes

$$\nabla_{\boldsymbol{\delta}} g(\boldsymbol{\theta}, \boldsymbol{\delta}^*(\boldsymbol{\theta})) + \mathbf{B}_0^\top \boldsymbol{\lambda}^*(\boldsymbol{\theta}) = \mathbf{0}, \quad \text{and} \quad \mathbf{B}_0 \boldsymbol{\delta}^*(\boldsymbol{\theta}) - \mathbf{b}_0 = \mathbf{0}, \quad (17)$$

where the nonzero $\boldsymbol{\lambda}^*(\boldsymbol{\theta})$ only corresponds to the active constraints. We take derivatives w.r.t. $\boldsymbol{\theta}$ of (17), and thus obtain the following

$$\begin{aligned} & \frac{d\nabla_{\boldsymbol{\delta}} g(\boldsymbol{\theta}, \boldsymbol{\delta}^*(\boldsymbol{\theta}))^\top}{d\boldsymbol{\theta}} + \nabla_{\boldsymbol{\theta}} \boldsymbol{\lambda}^*(\boldsymbol{\theta})^\top \mathbf{B}_0 = \mathbf{0} \\ \implies & \nabla_{\boldsymbol{\theta}\boldsymbol{\delta}} g(\boldsymbol{\theta}, \boldsymbol{\delta}^*(\boldsymbol{\theta})) + \underbrace{\frac{d\boldsymbol{\delta}^*(\boldsymbol{\theta})^\top}{d\boldsymbol{\theta}}}_{\text{IG}} \nabla_{\boldsymbol{\delta}\boldsymbol{\delta}} g(\boldsymbol{\theta}, \boldsymbol{\delta}^*(\boldsymbol{\theta})) + \nabla_{\boldsymbol{\theta}} \boldsymbol{\lambda}^*(\boldsymbol{\theta})^\top \mathbf{B}_0 = \mathbf{0}, \end{aligned} \quad (18)$$

$$\text{and} \quad \underbrace{\frac{d\boldsymbol{\delta}^*(\boldsymbol{\theta})^\top}{d\boldsymbol{\theta}}}_{\text{IG}} \mathbf{B}_0^\top = \mathbf{0}, \quad (19)$$

where $\nabla_{\boldsymbol{\theta}\boldsymbol{\delta}} \in \mathbb{R}^{|\boldsymbol{\theta}| \times |\boldsymbol{\delta}|}$ denotes second-order partial derivatives (recall that $|\boldsymbol{\theta}| = n$ and $|\boldsymbol{\delta}| = d$). According to (18), we have

$$\frac{d\boldsymbol{\delta}^*(\boldsymbol{\theta})^\top}{d\boldsymbol{\theta}} = -[\nabla_{\boldsymbol{\theta}\boldsymbol{\delta}} g(\boldsymbol{\theta}, \boldsymbol{\delta}^*(\boldsymbol{\theta})) + \nabla_{\boldsymbol{\theta}} \boldsymbol{\lambda}^*(\boldsymbol{\theta})^\top \mathbf{B}_0] \nabla_{\boldsymbol{\delta}\boldsymbol{\delta}} g(\boldsymbol{\theta}, \boldsymbol{\delta}^*(\boldsymbol{\theta}))^{-1}. \quad (20)$$

Substituting the above into (19), we obtain

$$\nabla_{\boldsymbol{\theta}\boldsymbol{\delta}} g(\boldsymbol{\theta}, \boldsymbol{\delta}^*(\boldsymbol{\theta})) \nabla_{\boldsymbol{\delta}\boldsymbol{\delta}} g(\boldsymbol{\theta}, \boldsymbol{\delta}^*(\boldsymbol{\theta}))^{-1} \mathbf{B}_0^\top + \nabla_{\boldsymbol{\theta}} \boldsymbol{\lambda}^*(\boldsymbol{\theta})^\top \mathbf{B}_0 \nabla_{\boldsymbol{\delta}\boldsymbol{\delta}} g(\boldsymbol{\theta}, \boldsymbol{\delta}^*(\boldsymbol{\theta}))^{-1} \mathbf{B}_0^\top = \mathbf{0}, \quad (21)$$

which yields:

$$\nabla_{\boldsymbol{\theta}} \boldsymbol{\lambda}^*(\boldsymbol{\theta})^\top = -\nabla_{\boldsymbol{\theta}\boldsymbol{\delta}} g(\boldsymbol{\theta}, \boldsymbol{\delta}^*(\boldsymbol{\theta})) \nabla_{\boldsymbol{\delta}\boldsymbol{\delta}} g(\boldsymbol{\theta}, \boldsymbol{\delta}^*(\boldsymbol{\theta}))^{-1} \mathbf{B}_0^\top [\mathbf{B}_0 \nabla_{\boldsymbol{\delta}\boldsymbol{\delta}} g(\boldsymbol{\theta}, \boldsymbol{\delta}^*(\boldsymbol{\theta}))^{-1} \mathbf{B}_0^\top]^{-1}, \quad (22)$$

and thus,

$$\nabla_{\boldsymbol{\theta}} \boldsymbol{\lambda}^*(\boldsymbol{\theta})^\top \mathbf{B}_0 = -\nabla_{\boldsymbol{\theta}\boldsymbol{\delta}} g(\boldsymbol{\theta}, \boldsymbol{\delta}^*(\boldsymbol{\theta})) \nabla_{\boldsymbol{\delta}\boldsymbol{\delta}} g(\boldsymbol{\theta}, \boldsymbol{\delta}^*(\boldsymbol{\theta}))^{-1} \mathbf{B}_0^\top [\mathbf{B}_0 \nabla_{\boldsymbol{\delta}\boldsymbol{\delta}} g(\boldsymbol{\theta}, \boldsymbol{\delta}^*(\boldsymbol{\theta}))^{-1} \mathbf{B}_0^\top]^{-1} \mathbf{B}_0. \quad (23)$$

Substituting (23) into (20), we obtain the IG

$$\begin{aligned} \frac{d\delta^*(\boldsymbol{\theta})^\top}{d\boldsymbol{\theta}} &= -\nabla_{\boldsymbol{\theta}\delta}g(\boldsymbol{\theta}, \delta^*(\boldsymbol{\theta}))\nabla_{\delta\delta}g(\boldsymbol{\theta}, \delta^*(\boldsymbol{\theta}))^{-1} - \nabla_{\boldsymbol{\theta}}\boldsymbol{\lambda}^*(\boldsymbol{\theta})^\top \mathbf{B}_0 \nabla_{\delta\delta}g(\boldsymbol{\theta}, \delta^*(\boldsymbol{\theta}))^{-1} \\ &= -\nabla_{\boldsymbol{\theta}\delta}g(\boldsymbol{\theta}, \delta^*(\boldsymbol{\theta}))\nabla_{\delta\delta}g(\boldsymbol{\theta}, \delta^*(\boldsymbol{\theta}))^{-1} \\ &\quad + \nabla_{\boldsymbol{\theta}\delta}g(\boldsymbol{\theta}, \delta^*(\boldsymbol{\theta}))\nabla_{\delta\delta}g(\boldsymbol{\theta}, \delta^*(\boldsymbol{\theta}))^{-1}\mathbf{B}_0^\top [\mathbf{B}_0 \nabla_{\delta\delta}g(\boldsymbol{\theta}, \delta^*(\boldsymbol{\theta}))^{-1}\mathbf{B}_0^\top]^{-1}\mathbf{B}_0 \nabla_{\delta\delta}g(\boldsymbol{\theta}, \delta^*(\boldsymbol{\theta}))^{-1}. \end{aligned} \quad (24)$$

The above completes the proof of Proposition 1. \square

To further compute (24), the Hessian matrix $\nabla_{\delta\delta}\ell_{\text{atk}}$ is needed. Recall from the definition of the lower-level objective that the Hessian matrix is given by

$$\nabla_{\delta\delta}g(\boldsymbol{\theta}, \delta^*(\boldsymbol{\theta})) = \nabla_{\delta\delta}\ell_{\text{atk}} + \lambda\mathbf{I} = \mathbf{0} + \lambda\mathbf{I}. \quad (25)$$

Here we used the assumption that $\nabla_{\delta\delta}\ell_{\text{atk}} = \mathbf{0}$. The rationale behind that is neural networks commonly leads to a piece-wise linear decision boundary w.r.t. the inputs [44, 45], and thus, its second-order derivative (Hessian) $\nabla_{\delta\delta}\ell_{\text{atk}}$ is close to zero.

Based on the simplification (25), we have

$$\begin{aligned} \frac{d\delta^*(\boldsymbol{\theta})^\top}{d\boldsymbol{\theta}} &= - (1/\lambda)\nabla_{\boldsymbol{\theta}\delta}g(\boldsymbol{\theta}, \delta^*(\boldsymbol{\theta})) \underbrace{\left(\mathbf{I} - \mathbf{B}_0^\top [\mathbf{B}_0 \mathbf{B}_0^\top]^{-1} \mathbf{B}_0\right)}_{:=\mathbf{H}_C} \\ &\quad - (1/\lambda)\nabla_{\boldsymbol{\theta}\delta}\ell_{\text{atk}}(\boldsymbol{\theta}, \delta^*(\boldsymbol{\theta}))\mathbf{H}_C, \end{aligned} \quad (26)$$

where we have used the fact that $\nabla_{\boldsymbol{\theta}\delta}g = \nabla_{\boldsymbol{\theta}\delta}\ell_{\text{atk}}$.

What is \mathbf{H}_C in (26)? Since $\mathbf{B} = \begin{bmatrix} \mathbf{I} \\ -\mathbf{I} \end{bmatrix}$, we can obtain that $\mathbf{B}_0 \mathbf{B}_0^\top = \mathbf{I}$ and $\mathbf{B}_0^\top \mathbf{B}_0$ is a sparse diagonal matrix with diagonal entries being 0 or 1. Thus, \mathbf{H}_C can be first simplified to

$$\mathbf{H}_C = \mathbf{I} - \mathbf{B}_0^\top \mathbf{B}_0. \quad (27)$$

Clearly, \mathbf{H}_C is also a diagonal matrix with either 0 or 1 diagonal entries. The 1-valued diagonal entry of \mathbf{H}_C corresponds to the *inactive constraints* in $\mathbf{B}\delta^*(\boldsymbol{\theta}) < \mathbf{b}$, i.e., those satisfied with *strict inequalities* in $\{\|\delta\|_\infty \leq \epsilon, \mathbf{0} \leq \delta \leq \mathbf{1}\}$. This can be expressed as

$$\mathbf{H}_C = [1_{p_1 \leq \delta_1^* \leq q_1} \mathbf{e}_1, \dots, 1_{p_d \leq \delta_d^* \leq q_d} \mathbf{e}_d] \quad (28)$$

where $1_{p_i \leq \delta_i^* \leq q_i} \in \{0, 1\}$ denotes the indicator function over the constraint $\{p_i \leq \delta_i^* \leq q_i\}$ and returns 1 if the constraint is satisfied, δ_i^* denotes the i th entry of $\delta^*(\boldsymbol{\theta})$, $p_i = \max\{-\epsilon, -x_i\}$ and $q_i = \min\{\epsilon, 1 - x_i\}$, and $\mathbf{e}_i \in \mathbb{R}^d$ denotes the basis vector with the i th entry being 1 and others being 0s.

Based on the definition of g , (26) and (28), we can eventually achieve the desired IG formula (13). The proof of Corollary 1 is now complete. \square

B Discussion on case $\ell_{\text{atk}} = -\ell_{\text{tr}}$

We provide an in-depth explanation on the fact that even if we set $\ell_{\text{atk}} = -\ell_{\text{tr}}$, the *optimization routine* given by (4) to solve problem (3) does not reduce to the ordinary IG-absent gradient descent to solve problem (1) because of the presence of lower-level constraints.

- In the **absence** of the constraint $\delta \in \mathcal{C}$, if we set $\ell_{\text{atk}} = -\ell_{\text{tr}}$, then solving problem (3) via IG-involved descent method (4) will reduce to the ordinary IG-absent method that solves problem (1).

This is a known BLO result (e.g. [35]) and can be readily proven using the stationary condition. To be specific, based on the stationary condition of unconstrained lower-level optimization, we have $\nabla_{\delta} \ell_{\text{atk}}(\boldsymbol{\theta}, \boldsymbol{\delta}^*) = 0$. Since $\ell_{\text{atk}} = -\ell_{\text{tr}}$, we have $\nabla_{\delta} \ell_{\text{tr}}(\boldsymbol{\theta}, \boldsymbol{\delta}^*) = 0$. As a result, the second term in (4) becomes 0 and solving problem (3) becomes identical to solving the min-max problem (1).

- In the **presence** of the constraint $\delta \in \mathcal{C}$, the stationary condition cannot be applied since the stationary point may not be a feasible point in the constraint. In other words, $\nabla_{\delta} \ell_{\text{atk}}(\boldsymbol{\theta}, \boldsymbol{\delta}^*) = 0$ does not hold in the case of $\ell_{\text{atk}} = -\ell_{\text{tr}}$. As a matter of fact, one has to resort to KKT conditions instead of the stationary condition for a constrained lower-level problem. Similar to our proof in Proposition 1, the implicit gradient (and thus the second term of (4)) cannot be omitted in general. This makes the optimization routine to solve problem (3) different from solving problem (1).

C Detailed Experiment settings

C.1 Training Set-up

For CIFAR-10, we summarize the training setup for each method. 1) FAST-AT: We use FGSM with an attack step size of 1.25ϵ to generate perturbations; 2) PGD-2-AT: 2-step PGD attacks¹ with an attack step size of 0.5ϵ is implemented; 3) FAST-AT-GA: The gradient alignment regularization parameter is set to the recommended value for each ϵ ; 4) FAST-BAT: We select λ from $255/5000$ to $255/2000$ for different ϵ . At the same time, we adjust α_2 accordingly, so that the coefficient of the second term in (14), namely α_2/λ always equals to $0.1\alpha_1$.

For ImageNet, we set ϵ to $2/255$, and we strictly follow the training setting adopted by [1]. In FAST-BAT, we fix λ at $255/3000$ and adopt the same α_2 selection strategy as CIFAR-10.

Parameter for FAST-AT-GA Regarding FAST-AT-GA with different model types, we adopt the same regularization parameter recommended in its official repo² intended for PreActResNet-18 (namely 0.2 for $\epsilon = 8/255$ and 2.0 for $\epsilon = 16/255$).

¹We use random initialization to generate perturbations for PGD, while in the paper of FAST-AT-GA [18], 2-step PGD is initialized at zero point, which we believe will underestimate the effect of PGD-2-AT

²FAST-AT-GA: <https://github.com/tml-epfl/understanding-fast-adv-training/blob/master/sh>

D Additional Experimental Results

We train DNN models ResNet (RN)-50 [49] for ImageNet and we choose the training perturbation strength $\epsilon = 2/255$ strictly following [1, 18]. We remark that when evaluating on ImageNet, we only compare ours with FAST-AT since as shown in Table 6 of [18], the other baseline methods did not show any improvement over Fast-AT at the attack budget $\epsilon = 2/255$. RA-PGD stands for the robustness against PGD-50-10 (50-step PGD attack with 10 restarts) with $\epsilon = 2/255$. Table A1 shows the performance comparison between FAST-AT and FAST-BAT. We can see FAST-BAT outperforms FAST-AT by 1.23% when facing attacks with $\epsilon = 2/255$.

Table A1: SA and RA on ImageNet.

Method	SA (%)	RA-PGD (%)
FAST-AT	60.90	43.43
FAST-BAT	60.18	44.64

Sensitivity to regularization parameter λ In Table A2, we show the sensitivity of FAST-BAT to the regularization parameter λ . All the parameters remain the same as the default setting, except that for different λ . We always adjust α_2 so that $\alpha_2/\lambda = 0.1\alpha_1$ holds. Note $1/\lambda$ also serves as the attack step in (9). As λ decreases, the improvement in robust accuracy is evidently strengthened, and there is an obvious trade-off between robust accuracy (SA) and standard accuracy (RA). At a certain level of λ , namely when $\lambda \leq 255/2000$, RA starts to converge and stop surging.

Table A2: Performance of FAST-BAT with different parameter λ . We train and evaluate with the same attack budget $\epsilon = 16/255$ on CIFAR-10 to show the influence brought by λ .

CIFAR-10, PreActResNet-18, $\epsilon = 16/255$					
$1/\lambda$ (/255)	500	1000	1500	2000	2500
SA (%)	83.20	75.06	69.31	67.81	67.59
RA-PGD (%)	19.02	21.42	23.34	26.07	26.12

Sensitivity to different α_2 choices We consider the case of robust training with the large ϵ choice (16/255). As we can see from Table A3, if α_2 is set too small ($\alpha_2 = 0.008\alpha_1$), then both SA and RA will drop significantly. Here α_1 is set as the cyclic learning rate and thus not a constant parameter. However, in the α_2 interval $[0.0125\alpha_1, 0.025\alpha_1]$, we observed a tradeoff between standard accuracy (SA) and robust accuracy (RA): That is, the improvement in RA corresponds to a loss in SA. In our experiments, we choose α_2 when the tradeoff yields the best RA without suffering a significant drop of SA (which still outperforms the baseline approaches).

Table A3: Performance of FAST-BAT with different α_2 choices on CIFAR-10. Models are trained and evaluated with the same attack budget ($\epsilon = 16/255$). Here α_1 is set as the cyclic learning rate and thus, is not a constant parameter. α_2 is always set proportionate to α_1 for simplicity.

α_2 (CIFAR-10, PreActResNet18, $\epsilon = 16/255$)	$0.025\alpha_1$	$0.0167\alpha_1$	$0.0125\alpha_1$	$0.008\alpha_1$
SA (%)	75.06	69.31	67.81	57.92
RA-PGD (%)	21.42	23.34	26.07	20.53

Sensitivity of linearization schemes Fast-BAT needs a good linearization point \mathbf{z} in (8). In experiments, we adopt the perturbation generated by 1-step PGD without sign as our default linearization scheme. In Table A4, we show the performance of the other possible linearization options. We find that 1-step PGD without sign achieves the best robust accuracy among all the choices. This is not spurring since this linearization point choice is consistent with the first-Taylor expansion that we used along the direction of the input gradient without the sign operation involved. By contrast, FAST-BAT linearized with uniformly random noise suffers from catastrophic overfitting and reaches a rather low standard accuracy (SA). FAST-BAT with other linearizations also yields a worse SA-RA trade-off than our proposal.

Table A4: Performance of FAST-BAT with different linearization schemes. Besides 1-step PGD without sign (**PGD w/o Sign**), we further generate linearization point with the following methods: uniformly random noise $[-\epsilon, \epsilon]^d$ (**Uniformly Random**); uniformly random corner $\{-\epsilon, \epsilon\}^d$ (**Random Corner**); and perturbation from 1-step PGD attack with 0.5ϵ as attack step (**PGD**).

CIFAR-10, PreActResNet-18, $\epsilon = 16/255$				
Linearization Method	PGD w/o Sign	Uniformly Random	Random Corner	PGD
SA (%)	69.31	43.42	62.19	75.30
RA-PGD (%)	23.34	21.25	16.5	19.42